



Experimental investigation on the low-yield-strength steel shear panel damper under different loading



Zhang Chaofeng^a, Aoki Tetsuhiko^b, Zhang Qiuju^a, Wu Meiping^{a,*}

^a School of Mechanical Engineering, Jiangnan University, China

^b School of Civil Engineering, Aichi Institute of Technology, Japan

ARTICLE INFO

Article history:

Received 14 October 2012

Accepted 30 January 2013

Available online 27 March 2013

Keyword:

Low-yield-strength steel

Static loading

Dynamic constant loading

Dynamic random wave loading

Hysteretic behavior

ABSTRACT

To evaluate the hysteretic behavior of the low-yield-strength steel shear panel damper (LYSPD) accurately is very important for the dynamic analysis of the structure. Various analytical models for hysteretic behavior of the LYSPD are based on the static experiment results nowadays while it may be affected by dynamic loading speed, loading history and increased temperature. This paper presents a series of static and dynamic experimental investigations for examining the hysteretic behavior of the LYSPD. Obvious difference is observed between static and dynamic hysteretic curves. The test results suggest that the precise description of the nonlinear behavior of the LYSPD under static loading makes no sense. The nonlinear behavior of the LYSPD is replaced by linear strain hardening caused by dynamic loading speed and the perfect elastic–plastic model is more suitable for describing the hysteretic behavior of the LYSPD under dynamic random wave.

© 2013 Elsevier Ltd. All rights reserved.

1. Introduction

Passive energy absorption damper is widely adopted in current seismic resistant design of structures [1–3]. In the design approaches, damper that is installed in the building or the bridge serves as a fixing apparatus under small earthquake while it plays an important role to dissipate energy during large earthquakes. The effective damper force is set lower than the structural yield force to prevent the failure of structure and it could be adjusted by the cross section or the number of the damper. The earthquake energy is mainly dissipated by the damper which works just like “fuse” and failures while the structure remains intact during the earthquake.

As the low-yield-strength steel (100 N/mm²) possesses the merits such as stable hysteresis curve, good low-cycle fatigue characteristics, insensitivity to the ambient temperature etc., it is an ideal material for the design of damper. Since the concept of structural vibration control is proposed in 1972 [4], theoretical and experimental research on the low-yield-strength steel and development of various dampers are made effort by many scholars in the world [5–12]. So far, the dampers made from low-yield-strength steel have been widely applied to the practical engineering of building and bridge in the United States, Japan, Canada, New Zealand and other countries.

No matter what kind of the damper shape, the cyclical plastic deformation of the low-yield-strength steel is used to absorb the seismic energy. Simultaneously, the energy absorption capacity is depended not only on the deformation capacity but also on the stable force of

the damper. And, it is very important to evaluate the energy absorption performance of the damper when the damper is incorporated into the structure. In view of that mentioned above, to set up a model that can well predict the hysteretic behavior of the damper under the seismic wave is an effective solution. And, a number of models that describe the hysteretic curves of the dampers have been proposed by several researchers [13–17]. As the low-yield-strength steel has no apparent yield strength, the hysteretic behavior of the damper is composed of elastic segment, perfect-plastic segment and the smooth transition segment from elastic to plastic in ordinary in which the latest segment is also needed to be modeled accurately. Among the models that describe the smooth transition, Ramberg–Osgood and Boun–Wen [18] models are usually adopted because the Baushinger effect as well as strain hardening and/or strain softening can both be incorporated into these two models. However, the numerical analysis are all based on the static test results, the dynamic behavior of the damper is still unclear. Therefore, it is necessary to organize dynamic tests to verify the feasibility of the models mentioned above or to set up a new rational model of the damper.

Nowadays, the series research on one LYSPD including static increment, static constant, dynamic constant and dynamic random wave is still rare. However, the series research on the damper is very valuable for the researchers to understand the damper performance systematically and it is also very important for the damper designers to grasp the real damper performance well. Therefore, one LYSPD with a 70% shear strain [horizontal displacement/height ($\gamma = \delta/H$)], verified to be the maximum deformation capacity of the LYSPDs at present [19], is selected as the test specimen firstly. Subsequently, serial tests are conducted to investigate the hysteretic behavior of the LYSPD under different loading. Results and discussions are presented, emphasizing

* Corresponding author. Tel.: +86 510 8591 0586.

E-mail address: wmp169@hotmail.com (M. Wu).

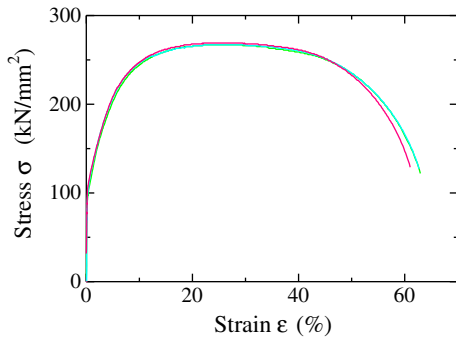


Fig. 1. Tensile coupon experiment results.

the key factors that affect the hysteretic behavior and setting up a rational numerical model for the LYSPD.

2. LYSPD

2.1. Performance of low-yield-strength steel

Tensile coupon tests for low-yield-strength steel 100 are conducted and the obtained stress–strain curves are demonstrated as Fig. 1. The yield strength σ_y defined by the 0.2% offset value of $\sigma_{0.2}$ is 100 N/mm² and the elongation reaches 60%. The yield shear stress is about 58 N/mm². The maximum stress is around 265 N/mm² and the corresponding maximum shear stress is around 155 N/mm². The curves can be nearly divided into four sections: the elastic section, smooth transition from elastic to plastic, the perfect plastic section and the degradation section.

2.2. LYSPD structural

The shape and size of the specimen are shown in Fig. 2(a). Ribs are widely applied to the design of shear panels or other structures for the purpose of improving the stress concentration located at the corners. However, the rib ends are easy to crack under the hysteretic loading with large shear angle due to the material deterioration resulting from welding. Moreover, the stress concentration at the panel's four corners is apt to be further intensified by welding intersections. Taking the above into consideration, two stiffeners ($t = 24 \text{ mm/h} = 50 \text{ mm}$) at the up and down sides of the panel are shaped after the original panel instead of by welding, whereby the local “plastic hinges” at the corners

of effective panel area are properly separated from the rib ends. To prevent the stress concentration caused by sharp variable cross-section, arcs of 47 mm radius are introduced to handle different panel thickness in connecting. The ribs are the thin panels made also from LYS100, 266 mm in length, 72 in width and 12 in thickness. The deformation capacity of the shear panel is thus enabled to reach 70% shear strain by the optimization.

As indicated by Fig. 2(b) and (c), with the LYSPD fixed on the base plate by 12 M24 high-strength bolts the top fixture can move freely in a horizontal line. The seismic function of the LYSPD could be recovered soon after the earthquake as it can be easily replaced or re-centered. The bending moment and the out-of-plane torsion of shear panel are suppressed by two pairs of links set at both sides of the panel. The link mechanism is made from SM490 and SS400.

3. Test detail

3.1. Test setup

As shown in Fig. 3, one head of the 100 t MTS dynamic actuator is fixed on the back strength wall and the other connected to the beam that can move horizontally. Two counterforce devices are installed on the beam to provide the force acting on the topside of the LYSPD.

In this experiment, force is measured through the actuator load cell (0.5 kN in precision) and displacement measured by laser extensometers (0.05 mm in precision). To eliminate the errors caused by test equipment to secure the accurate data of damper horizontal displacement, two laser extensometers (LEX1 and LEX2) are used to measure the horizontal displacement at the LYSPD's top and bottom beams. Difference in measuring results between LEX1 and LEX2 is taken as the pure horizontal displacement of the LYSPD. And the temperature of the LYSPD is detected in real time by non-contact temperature sensor TH6300R.

3.2. Test plan

The horizontal displacement/panel effective height is defined as shear strain γ . In the present study, a reversed cyclic loading controlled by the shear strain is applied to the specimens (see Fig. 4).

As shown in Fig. 4(a), the loading pattern is a stepwise incremental cyclic loading protocol adopted in the deformation capacity verification test of the development stage. The increment shear strain is 5%, the ultimate maximum shear strain is 70%.

The static and dynamic constant tests are presented by Fig. 4(b) and (c). The waveforms are applied with amplitudes of 20%, 30%,

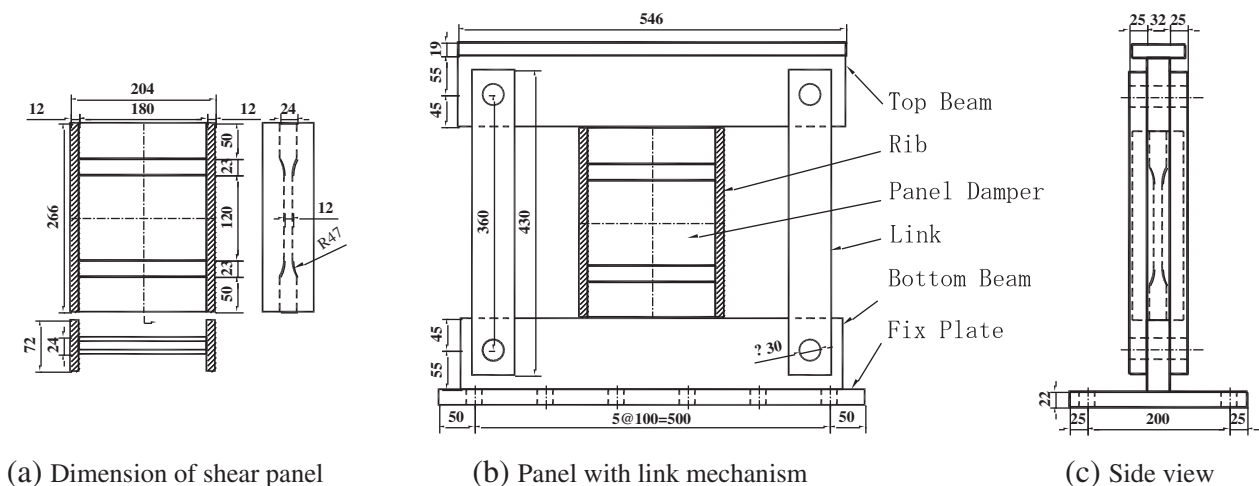


Fig. 2. Specimen details (units: mm).



Fig. 3. Test setup.

40% and 50% shear strain γ respectively. The cycles are fully reversed with strain ratio $R = \gamma_{min}/\gamma_{max} = -1$, varying just at shear strain amplitude γ and shear strain rate $\dot{\gamma}_v$. The shear strain rate $\dot{\gamma}_v$ of quasi-static loading is 0.4%/s (0.5 mm/s), 0.5 Hz and 1 Hz that represent the typical resonance frequencies of bridge systems are set as the dynamic loading frequencies [20].

Seismic response waves of the LYSPD are investigated through simulation on a bridge sample, which is a typical bridge in practical application and is an example in the DYMO software [21] developed by the Japan Civil Engineering Research Center and widely applied to the accurate dynamic analysis of bridge systems. The waves, recorded in Japan's 1995 Hyogoken Nanbu Earthquake with a large

peak ground acceleration (PGA) and defined as level 2 waves in *Specifications for Highway Bridges of Japan* [22], are selected as input earthquake waves in the numerical analysis. Three seismic response waves of the LYSPD that appear badly prone to damage under each soil condition in simulation are chosen as the input earthquake waves of dynamic random tests, as illustrated in Fig. 4(d)–(f). These waves can well reflect the real motions of the LYSPD during the earthquake and they are unified as the same maximum shear strain of 70%. Simultaneously, the maximum shear strain of the wave02 is adjusted to 50% and 80% proportionally. This group is set to determine the damage to the LYSPD at different shear strain amplitudes or rates. In addition, for the purpose of eliminating the influence of temperature and

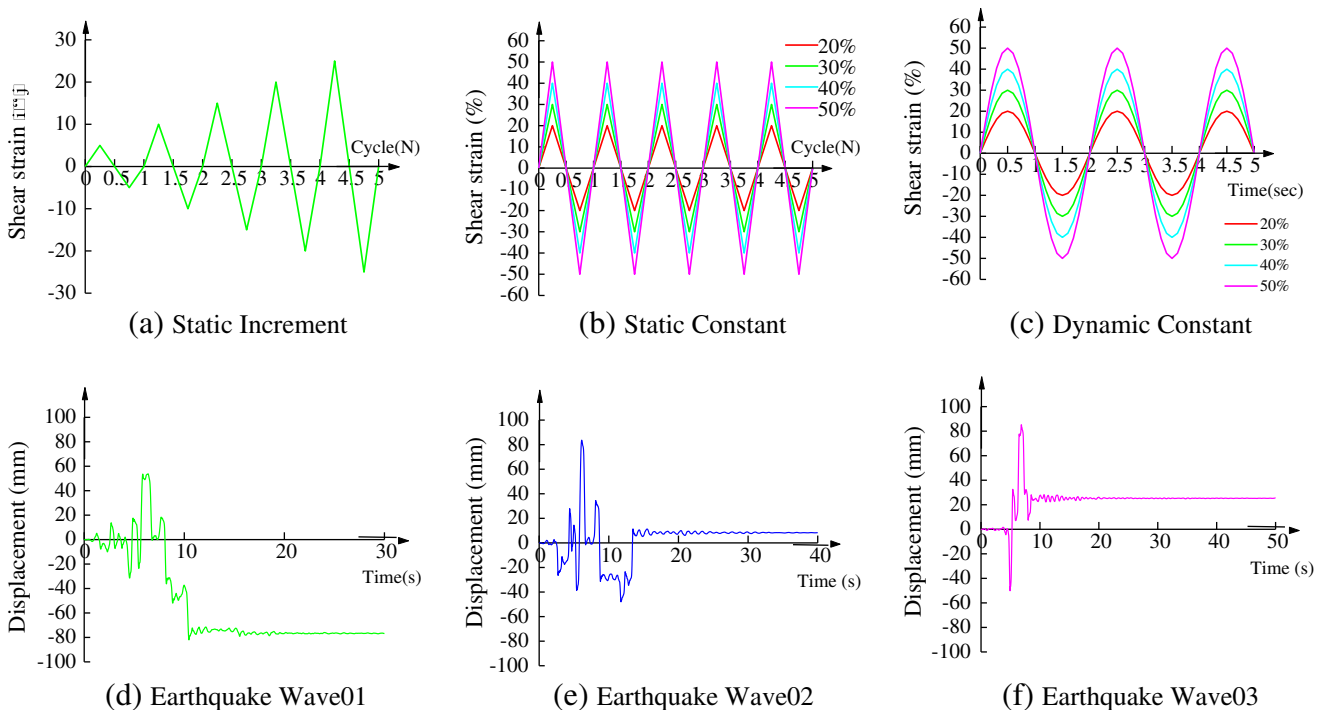


Fig. 4. Loading pattern.

Table 1
Test plan.

Loading pattern	Serial	Specimen	f (Hz)	T (s)	γ (%)	γ_v (%/s)	
Increment	Static	Inc70	–	–	70	0.4	
	Constant	Static (ST)	ST20	–	–	20	0.4
ST30					30		
ST40					40		
ST50					50		
D05-20			0.5	2	20	40	
Dynamic (D05)		D05-30			30	60	
		D05-40			40	80	
		D05-50			50	100	
		Dynamic (D10)	D10-20	1.0	1	20	80
			D10-30			30	120
D10-40				40	160		
D10-50				50	200		
Random	Wave01	W01-70	–	–	70	–	
	Wave02	W02-70					
	Wave03	W03-70					
	Wave02	W02-50			50		
	Wave02	W02-80			80		

residual displacement, re-centering and cooling follow the seismic response wave loading. And this process is repeated until the failure of the LYSPD. The test plan is listed in Table 1.

4. Results and discussion

4.1. Failure mode

Typical failure modes of the static and dynamic tests are shown in Fig. 5. With the increase of rotation angle (local bending) and hysteretic

tension and compression, at 60% loading shear strain, two small cracks of the welding seams and small rib necking are observed at the bottom “plastic hinges”. The welding seams and rib go totally broken at 70% loading shear strain. At the same time, small out-of-plane shear buckling is observed, as shown in Fig. 5(a). Representative constant static and dynamic failure mode at 30% loading shear strain is demonstrated in Fig. 5(b) and (c). In spite of the rarely small width/thickness ratio of the LYSPD, obvious out-of-plane shear buckling is observed in the static constant test (Fig. 5(b)). Instead of shear buckling in static constant tests, in-plane shear deformation is dominant in the dynamic constant tests (Fig. 5(c)). In the constant dynamic tests, a significant heat rise prior to failure is also observable within the effective panel-deformation area. The horizontal high-temperature red band is mainly caused by the horizontal layer internal friction triggered by in-plane simple shear. Similarly, the failure modes of the specimens in the dynamic random wave tests which undergo several same seismic waves are also resulting from the in-plane simple shear (Fig. 5(d)). And, as the same loading amplitude cannot be repeated in real seismic wave and coupled with the reduction of cycle number, the high-temperature red shear band in constant dynamic tests is not observed in the dynamic random wave tests. The panel cracks from the rib ends, followed with out-of-plane buckling.

As the out-of-plane shear buckling is observed in the static test of the LYSPD, the formation of the tension zone and the angle of the tensile are taken into the consideration of the maximum shear strength evaluation in the traditional researches. Meanwhile, instead of the out-of-plane shear buckling, the in-plane deformation is the dominant in the dynamic constant or random wave tests. The point defects induced by cross slips based on out-of-plane shear buckling are replaced by the in-plane interlaminar slips that parallel to the shear force. The in-plane interlaminar deformation has many

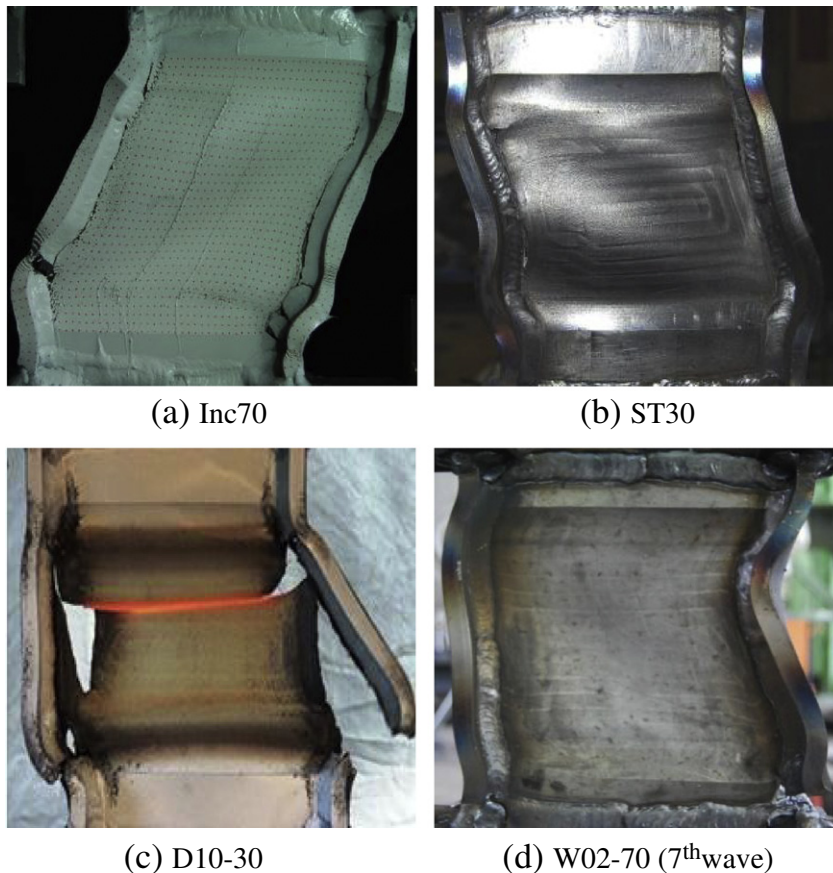
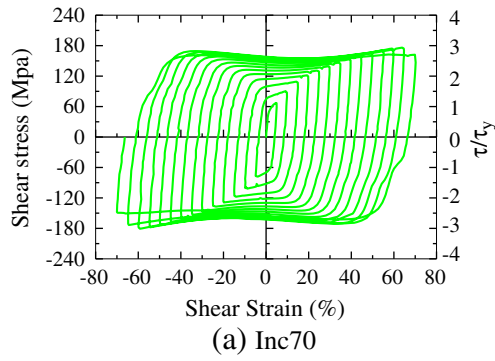
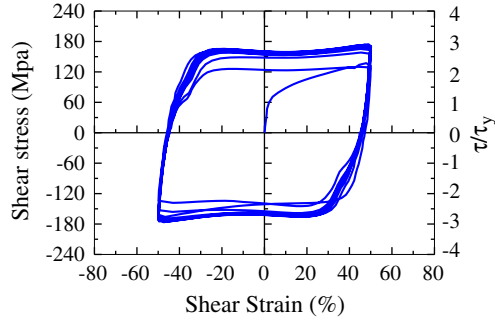


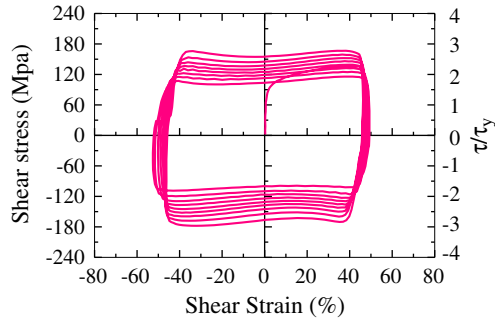
Fig. 5. Failure mode.



(a) Inc70



(b) ST50



(c) D05-50

Fig. 6. Representative hysteretic curves.

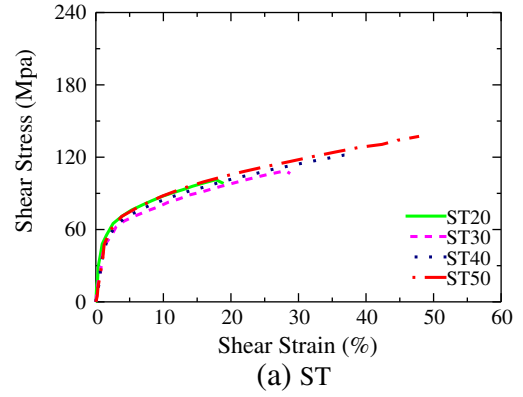
advantages, like the simplicity of the sample geometry, the absence of any plastic instability such as localization and/or necking in tension or barreling in compression, and the large range of achievable homogeneous strains. Therefore, the relation between shear stress and shear force can be simplified as:

$$F = \tau \cdot A \tag{1}$$

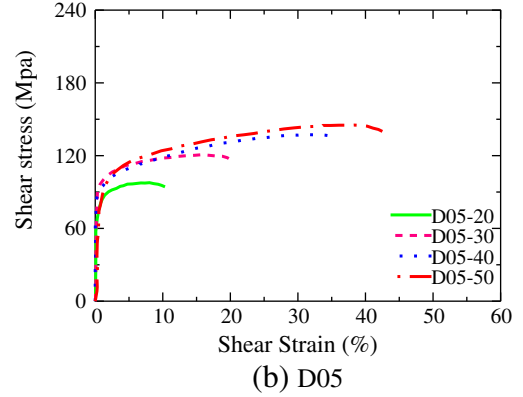
where F indicates the shear force, and A the shear area including the rib cross section. When the low-yield-strength steel is supposed as perfect elastic–plastic model, the shear stress τ can be expressed as,

$$\begin{cases} \tau = G\gamma & (0 < \gamma < \gamma_y) \\ \tau = \tau_y & (\gamma > \gamma_y) \end{cases} \tag{2}$$

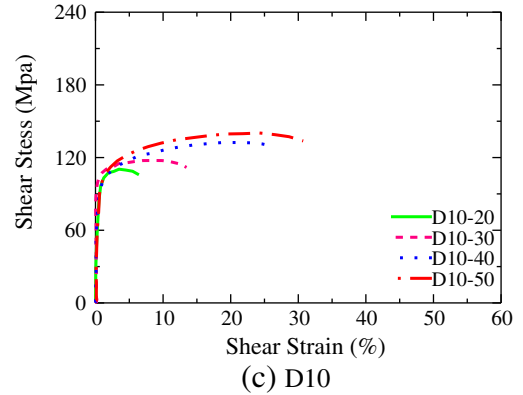
where, G indicates the shear elastic modulus, τ_y the yield shear stress, γ the shear strain, and γ_y the yield shear strain.



(a) ST



(b) D05



(c) D10

Fig. 7. Static and dynamic hysteretic curves in virgin stage.

4.2. Static and dynamic constant tests

4.2.1. Hysteretic curves

The hysteretic curve difference between static and dynamic constant tests is compared based on the test results preliminarily. The hysteretic curves of static increment test, static constant test and the representative hysteretic curve of dynamic constant test are shown in Fig. 6. The shape of the hysteretic curves in the static tests exhibits as spindle (Fig. 6(a) and (b)). And, the hysteretic curve is composed of elastic and smooth nonlinear curve when the shear strain amplitude is small. With the increase of the loading amplitude, an approximate perfect-plastic curve follows the curves mentioned above, as demonstrated in Fig. 6(a). Characterized with the Bauschinger effect, the shape of the static constant hysteretic curves (Fig. 6(b)) exhibits the same shape of the static increment hysteretic curve. However, the shape of the hysteretic curves in the dynamic constant tests exhibits

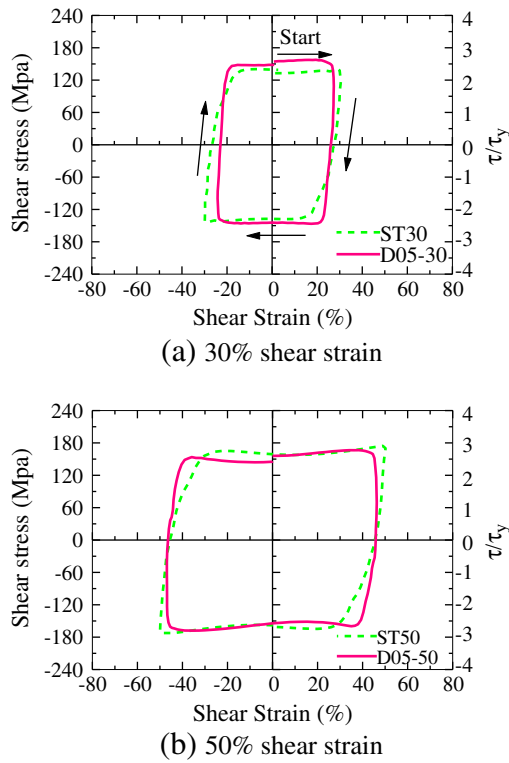


Fig. 8. Comparison of static and dynamic hysteretic curves.

as rectangular without the Bauschinger effect, as shown in Fig. 6(c). Large difference of hysteretic behavior between static tests and dynamic constant tests is observed according to the test results.

4.2.2. Virgin loading

The shear stress–shear strain curves under the virgin loading of static and dynamic constant tests are shown in Fig. 7. As the low-yield-strength steel possesses the good stability, four static test results with different response shear strains show the same hysteretic curve trajectory, as demonstrated in Fig. 7(a). It is composed of three parts, the elastic segment, the smooth transition from elastic to plastic and the plastic segment. The shear modulus G_{Est} , yield shear strain γ_{yst} and yield shear stress τ_{yst} of elastic segment are 38 kN/mm^2 , 1.2% and 47 kN/mm^2 respectively. The plastic segment is also demonstrated as linear with a plastic shear modulus around 1.3 kN/mm^2 . In the case of dynamic tests, the yield shear stresses are all around 2 times of the value of static test. Furthermore, the yield shear strains under dynamic tests are only half of that of the static tests. Based on these two points, the elastic shear modulus under dynamic tests G_{Edy} is about 4 times of that of the static tests. Simultaneously, under dynamic tests, the smooth transition segment between elastic and plastic is narrowed to a rarely small range and the plastic shear modulus G_{Pdy} drops 25% of that of the static tests. Therefore, the relation between static hysteretic curves and dynamic hysteretic curves can be described as follows,

$$G_{Edy} = G_{Est} f_1 (G_E, v_\gamma) \tag{3}$$

$$\gamma_{ydy} = \gamma_{yst} f_2 (\gamma, v_\gamma) \tag{4}$$

$$G_{Pdy} = G_{Pst} f_3 (G_E, v_\gamma) \tag{5}$$

where, f_1 is 4, regardless of speed changes (from 60%/s to 200%/s). f_2 and f_3 are 0.5 and 0.75 respectively. It is generally regarded that these changes are caused by the loading speed. Without the influence

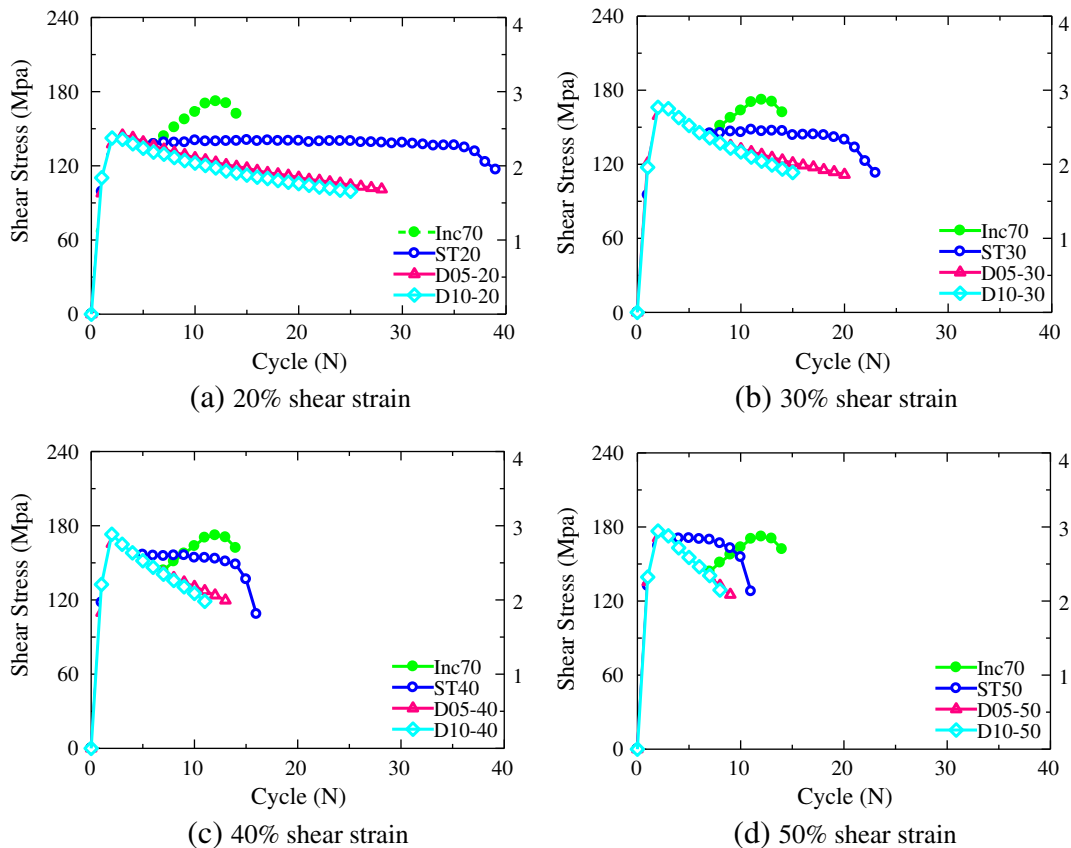


Fig. 9. Maximum stress history.

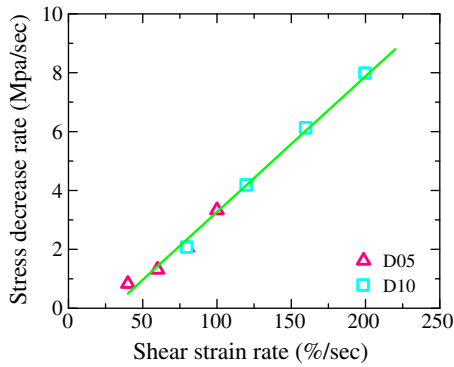


Fig. 10. Stress softening.

of loading history in the virgin loading, the viscous effect results from loading speed (stress hardening) is larger than the temperature effect (stress softening) results from plastic deformation. With the reduction of the yield shear strain and smooth transition of static hysteretic curves, the hysteretic curves under dynamic tests tend to the perfect elastic–plastic.

4.2.3. Cyclical loading

At the end of first cycle, the LYSPD reaches each maximum stress and begins the second cycle [23], as demonstrated in Fig. 8. Romberg–Osgood and Bouc–Wen models that can well describe the smooth curve of the Bauschinger effect are adopted by many scholars. The description of the smooth curve shape is realized by adjusting two shape parameters or four shape parameters in these two models respectively. However, the change of the hysteretic curve under the

dynamic loading has not been investigated or incorporated into these models.

Similar with the virgin loading, the elastic shear modulus is increased to about four times of that of the static test. In addition, the smooth transition between elastic and plastic segments in the static hysteretic curve is rectified to a linear relation. The Bauschinger effect no longer exists and the hysteretic curve can be modeled as perfect elastic–plastic model. As mentioned above, the dynamic loading plays a shaping role. The irregular nonlinear hysteretic curves under static test are reshaped as regular linear hysteretic curves.

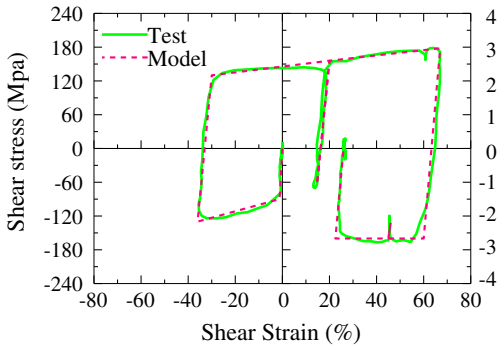
4.2.4. Stress history

A precise description of the smooth transition of the hysteretic curve becomes unimportant in the dynamic constant loading. Instead, based on the perfect elastic–plastic model, to clarify the cyclical stress hardening or stress softening caused by loading speed is hoped to arouse attention. As the isotropic hardening is observed in both static tests and dynamic tests, the positive maximum stress history in each cycle of the LYSPD is applied to analysis, as demonstrated in Fig. 9.

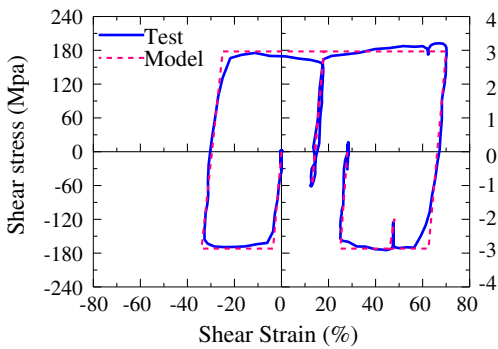
Affected by the loading speed, the maximum stresses of dynamic tests are larger than that of static tests, especially when the shear strain is 30% and 40%. The stress hardening should be paid attention to in the structure seismic design as the design approach relies on the bound force of the LYSPD. The maximum shear force of the LYSPD should be set lower than the yield force of main structure, and then the earthquake energy can be dissipated by the plastic deformation of the LYSPD. However, the stress hardening of the damper will trigger the malfunction of this mechanism, resulting in inadequate energy dissipation capacity of the damper and destruction of the main structure.

The maximum shear stress τ_{max} both in static and in dynamic tests is around 180 Mpa which is approximate with the value calculated based on the coupon test. It shows the feasibility that the stress of the LYSPD in the large plastic deformation can be calculated by Eq. (1) on the basis of homogeneity deformation supposition. The maximum shear stress is achieved and kept as a constant when the shear strain is larger than 50% in static tests. Affected by the stress hardening, the maximum shear stress is nearly approached when the shear strain is 30% in dynamic tests. As the deformation capacity of the LYSPD is more than 70% shear strain, the response amplitude of the LYSPD larger than 30% shear strain will be designed as the dominant energy absorption range in practical use. And the maximum shear stress can also be taken as the plastic stress in the perfect elastic–plastic model approximately.

With the increase of the cycle number, stress softening is easy to be produced which is greatly depended on the loading history and temperature. As shown in Fig. 9, when the same shear strain is repeated in dynamic tests, the stress softening is observed even when the increased temperature is not so high (Fig. 9(a)). That is, the shear band has been formed through the former shear loading. Without the enough time for the recovery of the crystal nucleation in the shear band, the crystal resist force in the LYSPD will decline in the next shear loading, especially when the same shear strain amplitude is repeated that acted on the LYSPD in the dynamic tests.



(a) First loading



(b) Second loading

Fig. 11. Hysteretic curve of W03-70.

4.3. Modeling

The hysteretic behavior of the LYSPD in the first cycle can be modeled as elastic–plastic relation with a small plastic modulus while it can be taken as perfect elastic–plastic relation from the second cycle. It can be expressed as:

$$\text{Virgin loading: } \begin{cases} \tau_{dy1} = G_{E dy} \cdot \gamma_{y dy} & \gamma < \gamma_{yd}; \\ \tau_{dy1} = G_{E dy} \cdot \gamma_{y dy} + G_{p dy} \dot{\gamma} & \gamma \geq \gamma_{yd}; \end{cases} \quad (6)$$

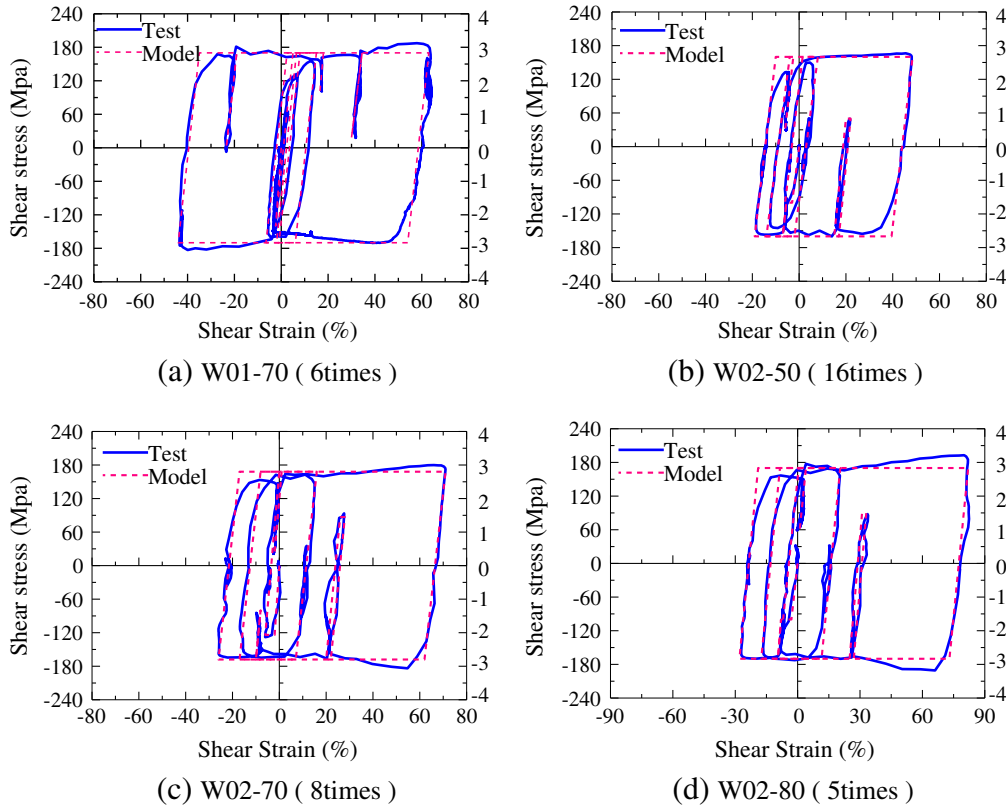


Fig. 12. Hysteretic curves of seismic wave.

$$\text{First reverse : } \begin{cases} \tau_{dy2} = G_{Edy} \cdot \gamma_{y1dy} & \gamma < \gamma_{y1dy} \\ \tau_{dy2} = G_{Edy} \cdot \gamma_{y1dy} + G_{p2} \gamma & \gamma \geq \gamma_{y1dy} \end{cases} \quad (7)$$

$$\text{Cycle : } \begin{cases} \tau_{dy} = K_s(\gamma, T(t)) \cdot G_{Edy} \cdot \gamma_{y2dy} & \gamma < \gamma_{y2dy}; \\ \tau_{dy} = \tau_{\max} & \gamma \geq \gamma_{y2dy}; \end{cases} \quad (8)$$

where $\dot{\gamma}$ indicates the strain increase, G_{p2} the plastic shear modulus after the first reverse, and K_s the stress softening factor.

In the initial reverse loading, whether it is the static test or the dynamic test, the maximum shear stress is achieved when the shear strain is 50%. Therefore, the maximum stress at 50% shear strain can be taken as an endpoint in the coordinate of the hysteretic curve. From the first reversal point, the hysteretic curve always moves straight to this endpoint. And then, the G_{p2} in Eq. (7) can be calculated

$$\text{as } G_{p2} = \frac{(\tau_{\max} - \tau_{dy1})}{(50\% - \gamma_{y1})}.$$

From the second cycle, the hysteretic curve exhibits as perfect elastic–plastic (Eq. (8)). The stress softening results from loading history or the temperature may be taken into the consideration of the modeling. In the dynamic constant tests, the loading history changes regularly and the loading speed is a constant. It makes the temperature increase as a constant speed. Under this circumstance, the stress decreases linearly with the loading speed, as illustrated in Fig. 10. The relation can be expressed as:

$$\tau_v = 0.17\gamma_v - 4.8. \quad (9)$$

However, there is small number of large shear strain responses which is also separated by several small shear strain responses in the seismic wave. The response of the LYSPD in the dynamic random wave is a benefit for the temperature dissipation and the influence of the stress softening is still to be discussed.

4.4. Seismic wave test

4.4.1. Difference between the first wave loading and the second wave loading

The response of wave03 is taken as the representative hysteretic curve to clarify the difference between the first wave loading and the second wave loading, as demonstrated in Fig. 11. The hysteretic behavior of the LYSPD under seismic loading can be modeled as the proposed elastic–plastic model or the perfect elastic–plastic model. The plastic shear modulus is observable in the first loading of the wave for the existence of the strain hardening and cyclical hardening while it is 0 in the second loading of the wave.

4.4.2. Stable response of the LYSPD

Except the W03-70 mentioned above, the hysteretic curves of the second loading of the other waves are taken as the typical curves and shown in Fig. 12. The failure numbers of the seismic waves are also listed in each title.

It is reported that the hysteretic behavior of the low-yield-strength steel damper can be precise as predicted by the perfect elastic–plastic model when the response shear strain is large while the error is not negligible when the response shear strain is small in the static tests [8]. The same phenomenon can also be observed in the dynamic tests with higher precision of evaluating the energy absorption. As shown in Fig. 12(a) and (b), when the response amplitude and the response speed of the LYSPD are both small, the hysteretic curve under seismic loading is similar with that of under static loading. However, the change of the hysteretic curve is observed when the maximum response amplitude of the LYSPD is proportionally expanded from 50% to 70% (Fig. 12(c)) and 80% (Fig. 12(d)). The nonlinear characteristic of the hysteretic curve (Fig. 12(b)) turns into perfect elastic–plastic behavior (Fig. 12(c),(d)). In addition, the damper can endure 5 times of the W02-80 which shows enough safety margins. In term of the full and

effective utilization of the LYSPD, the perfect elastic–plastic behavior will be the main characteristic of the hysteretic curves. On the other hand, the maximum shear strain of the traditional damper is not more than 30%. Based on the static test results, it is necessary to evaluate the insufficient energy absorption caused by nonlinear characteristic of the hysteretic curve for the security of the structure. However, even that the nonlinear exists in the small shear strain range (Fig. 12(a)), it has rarely a small influence on the energy evaluation based on perfect elastic–plastic model, because the earthquake energy is mainly absorbed by the large plastic deformation of the LYSPD. Therefore, the precise description of the nonlinear characteristic of the hysteretic curve when the response shear strain is small under the seismic loading has no meaning. The perfect elastic–plastic model is preferred as it is a simple and convenient model for design and practical application.

As has already been noted, this study also focuses on the response characters of the LYSPD under level-2 serve earthquake. The hysteretic cycles with large shear-strain amplitude in the LYSPD earthquake response waves are not more than 3 in general, the stress softening is not observed in all of the seismic waves before the failure of the LYSPD. Even that the maximum response shear strain in the W02-80 is 80% which also represents the maximum loading speed in all the seismic tests, the increased temperature is around 120 °C at the end of the 25 seconds' seismic wave. Meanwhile, the temperature climbed to 550 °C within 10 s in D10-50. Relative to the dynamic random test, the temperature effect is exaggerated by dynamic constant tests at least 20 times. Therefore, temperature rise has little to do with LYSPD model, which could thus be approximately evaluated by perfect elastic–plastic without the consideration of stress softening.

However, with more hysteretic response cycles, even under small plastic-strain amplitude, the LYSPD's stress softening should be given sufficient attention. For example, during the 2011 Japan Northeast Earthquake, the vibration lasts more than 1 min though its amplitude is not very large. Under this circumstance, the LYSPD stress softening is supposed to be evaluated by dynamic constant tests, which make our next research topic.

5. Conclusion

Serials of static and dynamic tests are conducted to investigate the hysteretic behavior of the developed LYSPD. Obvious difference between static tests and dynamic tests is observed and our major findings are summarized as follows:

- (1) The failure mode of the developed LYSPD under static constant tests is out-of-plane shear buckling while it is in-plane shear under dynamic constant and dynamic random wave tests.
- (2) The maximum shear force of the LYSPD can be calculated by maximum shear stress and the cross section area approximately on the basis of homogeneity deformation supposition.
- (3) Desirable stability and fine symmetry in two loading directions are exhibited by the hysteretic curves in all tests except the dynamic constant ones with stress softening.
- (4) Except the first random wave resulting from the virgin loading, the hysteretic curves of the LYSPD from the second random wave are all same which shows the perfect reusability and good stability.
- (5) A precise description of the smooth transition of the hysteretic curves in the static loading becomes unimportant in the

dynamic constant and random wave loading. Instead, attention should be paid to the change of elastic and plastic modulus.

- (6) The hysteretic behavior of the LYSPD under the dynamic random wave loading can be well predicted by the perfect elastic–plastic model without consideration of nonlinear.
- (7) The temperature-induced stress softening is negligible in the seismic response of the LYSPD in this research while it should be given sufficient attention to some special cases.

Acknowledgment

The authors thankfully acknowledge the full support given by the staff of Aichi Institute of Technology Seismic Research Center in Japan.

References

- [1] Tanaka Kiyoshi, Sasaki Yasuhiro, Yoneyama Shin-ichiro. An experimental study on hysteretic performance of shear panel dampers using different strength type of steel under static loading. *J Struct Constr Eng AIJ* 1999;520(6):117–24 [In Japanese].
- [2] Chan Ricky WK, Albermani Faris, Williams Martin S. Evaluation of yielding shear panel device for passive energy dissipation. *J Constr Steel Res* 2009;65:260–8.
- [3] Li Zhengying, Albermani Faris, Chan Ricky WK, Kitipornchai S. Pinching hysteretic response of yielding shear panel device. *Eng Struct* March 2011;33(3):993–1000.
- [4] Yao JTP. Concept of structure control. *J Struct Div ASCE* 1972;98(7):1567–74.
- [5] Skinner RI, Kelly JM, Heine AJ, et al. Hysteresis dampers for the protection of structures from earthquakes. *Bull N Z Soc Earthq Eng* 1980;13(1):22–6.
- [6] Hitomi Yasuyoshi, Wada Shinzo, Konomi Hatsunobu, Satito Kiichirou, Nakata Yasuhiro, Iwata Mamoru. Development of the high ductile shear panel. *Journal of AIJ* 1996;12:118–23 [In Japanese].
- [7] Kiyoshi TANAKA, Yasuhiro SASAKI. Hysteretic performance of shear panel dampers of ultra low yield-strength steel for seismic response control of buildings. The 12th World Conference on Earthquake Engineering (12WCEE); 2000. p. 1–8.
- [8] De Matteis G, Landolfo R, Mazzolani FM. Seismic response of MR steel frames with low-yield steel shear panels. *Eng Struct* 2003;25:155–68.
- [9] Ming-hsiang SHIH, Wen-pei SUNG, Cheer-germ GO. Investigation of newly developed added damping and stiffness device with low yield strength steel. *J Zhejiang Univ Sci* 2004;5(3):326–34.
- [10] Tateishi Kazuo, Hanji Takeshi, Minami Kuniaki. A prediction model for extremely low cycle fatigue strength of structural steel. *Int J Fatigue* 2007;29:887–96.
- [11] Dusicka Peter, Itani Ahmad M, Buckle Ian G. Cyclic response of plate steels under large inelastic strains. *J Constr Steel Res* 2007;63:156–64.
- [12] Aoki T, Dang J, Zhang C, Takaku T, Fukumoto Y. Dynamic shear test of low-yield steel panel dampers for bridge bearing. *STESSA* 2009:647–52.
- [13] Iwan WD. On a class of models for the yielding behavior of continuous and composite systems. *Trans ASME* 1967;89:612–7.
- [14] Dafalias YF, Popov EP. Plastic internal variables formalism of cyclic plasticity. *J Appl Mech ASME* 1976;43:645–51.
- [15] Jain AK, Geol SC, Hanson RD. Hysteretic cycles of axially loaded steel members. *J Struct Eng ASCE* 1980;106:1777–95.
- [16] Azizinamini A, Radzimirski JB. Static and cyclic performance of semirigid steel beam-to-column connections. *J Struct Eng ASCE* 1989;115:2979–99.
- [17] Nakashima M, Akazawa T, Tsuji B. Strain-hardening behavior of shear panels made of low-yield steel. II: model. *J Struct Eng ASCE* 1995;121:1750–7.
- [18] Ramberg W, Osgood WR. Description of stress–strain curves by three parameters. *NACA Tech Note* 1943;902.
- [19] Zhang Chaofeng, Zhang Zhisheng, Shi Jinfei. Development of high deformation capacity low yield strength steel shear panel damper. *J Constr Steel Res* 2012;75:116–30.
- [20] Japan Road Association. 2. 1996 Seismic design specifications of highway bridges; 1996.
- [21] Public Works Research Center. Manual of dynamic seismic design for highway bridges; 2006.
- [22] Japan Road Association. Specifications for highway bridges part V: seismic design; 2000.
- [23] Zhang Chaofeng, Zhang Zhisheng, Zhang Qiuju. Static and dynamic cyclic performance of a low-yield-strength steel shear panel damper. *J Constr Steel Res* 2012;79:195–203.